Supplemental Material: Failure Mechanisms of Air Entrainment in Drop Impact on Lubricated Surfaces

Min Pack[1], Han Hu[1], Dong-Ook Kim[1], Zhong Zheng[2], Howard A. Stone[2], and Ying Sun[1,*]

[1]*Department of Mechanical Engineering and Mechanics, Drexel University, Philadelphia, PA*

[2]*Department of Mechanical and Aerospace Engineering, Princeton University, Princeton, NJ*

1. TIRM-RIM methodology

Throughout our experiments, drops of various sizes (0.4-1.1 mm) were produced with a syringe pump (New Era, NE-300) and a custom-built piezoelectric drop generator of varying nozzle sizes. These drops were released onto lubricated glass substrates where the impact phenomenon was observed via high-speed imaging both by conventional side-view imaging and by a dual TIRM-RIM technique where the side-view camera was synchronized to the TIRM or RIM signals. The side view allows us to understand the morphological behavior of the drop impact with respect to time relative to the bottom view provided by the TIRM-RIM technique. The TIRM and RIM techniques provide the impact phenomenon close to the air and liquid interface which allows us to directly observe how the interstitial air layer between the droplet and the liquid film influences the drop impact conditions with $\approx 1\,\mathrm{nm}$ resolution in the *z*-direction and $\approx 20\,\mu\mathrm{s}$ temporal resolution.

Two high-speed cameras were synchronized to capture both the side view (Edgertronic) and the bottom view (Phantom, V711) of impacting drops as shown in fig. 1(a). The Edgertronic camera was used to capture the side-view images at 10,000 fps with a shutter speed of 1/200,000 s^{-1} using a 55 mm Nikon lens. A halogen light source (Dolan-Jenner) illuminated the drop from the side. The Phantom camera connected to a Navitar 12x objective was used to capture the TIRM images at 50,000 fps at 1 μs exposure times. The phantom camera was also used to measure the interferometry signals at 50,000 fps at 10 μs exposure times and was connected to a Proximity series Infini-Tube long objective with a 4x magnification. Needles of known radii were used to produce the scale bars in our experiments.

* Corresponding author. Tel.: +1(215)895-1373; Fax: +1(215)895-1478; E-mail:ysun@coe.drexel.edu.

1.1 TIRM background

As light travels through a medium, the incident light is bifurcated as reflected and refracted components. At a critical incident angle, the light is totally internally reflected. When light is totally internally reflected, an electromagnetic field with an exponentially decaying intensity known as the evanescent wave is generated into the less dense medium, for instance, air or water on a glass surface. The bottom view provided the total internal reflection microscopy (TIRM) imaging where a collimated light source (ThorLabs, M660) provided an angle of $\approx 45^{\circ}$ and thereby produced an evanescent wave with a decay length δ determined by $d = l / (4pn_1\sqrt{\sin^2 q_1 - (n_2 / n_1)^2}) » 136.7$ nm on top of an oil film on a glass slide optically coupled (Zeiss, Immersol 518f) on a BK7 dove prism (ThorLabs, PS993 and PS913) where λ is the wavelength of the light source, θ_1 is the incident angle (49.92°), n_1 and n_2 are the indexes of refraction of silicone oil and air respectively [1]. The critical contact angle for total internal reflection is calculated to be $\theta_c = \sin^{-1}(n_2 / n_1)$. The incident angle is greater than the critical angle for the oil and air interface $\theta_c^{\text{oil/air}} \approx 45.58°$, but less than the critical angle for the oil and water interface $\theta_c^{\text{oil/water}} \approx 71.80°$ which provides a grayscale contrast between the air-oil interface and a completely dark contrast between the water-oil interface. The air film thickness is then calculated by the following logarithmically decaying relationship $h = -d\log(1 - I(r,z,t) / I(r,z,0))$, where $I(r,z,t)$ is the local grayscale intensity normalized by the initial grayscale intensity $I(r,z,0)$ at t = 0 [1]. The images obtained via TIRM were naturally skewed and were stretched back the aspect ratio of 1 via post processing on ImageJ.

1.2 RIM background

Interferometry utilizes the fact that when the incident light is reflected between two interfaces, the superposition of two waves at any point – based on their constructive or destructive phases – dictates whether or not they reinforce or cancel each other causing bright or dark fringes. This phenomenon is perhaps most commonly observed via Newton's rings for light passing through a lens resting on a flat planar surface where the increase in air film thickness results in the spacing between fringes to decrease. This is due to the fact that the fringe-to-fringe spacing correlates to an air film thickness differential of $\lambda/2$, where λ is the wavelength of the light. For a resting lens, the zeroth dark fringe would be the fringe located where the radial dimension is zero

and the absolute air film thickness is known (mainly zero at the zeroth fringe). For an impacting droplet, such absolute thickness is unknown until contact is made for monochromatic light sources and this is where either dual-wavelength or color interferometry techniques[2,3] have been used in the past to obtain an absolute air film thickness. However, in our study, the issue of absolute thickness is overcome by juxtaposing the interferometry-derived air bubble or dimple to the evanescence-wave generated air film morphology. A collimated light source is again used for interferometry, the wavelength of the light naturally dictates the *z*-resolution corresponding to the fringe-to-fringe spacing (ThorLabs, M455). The air film morphology is determined in two steps. For one, a damped intensity trace represents a monotonically increasing air film thickness as in the spherical lens case in the Newton's ring generation and an increasing intensity trace represents a monotonically decreasing air film thickness. Secondly, the intensity trace is used to relate the intensity of the fringes to the air film thickness, *h*, by the following relationship $\left[2I-\left(I_{\max}+I_{\min}\right)\right]/(I_{\max}-I_{\min})=\cos\left(4\pi ih/\lambda+\pi\right)$ where I represents the grayscale intensity, $I_{\max}$ and $I_{\min}$ represent the maximum and minimum grayscale intensities respectively which are determined by a polynomial fitting, *i* represents the ith fringe from the zeroth fringe which is determined via TIRM in our experiments [2,4].

1.3 TIRM and RIM calibration

To calibrate the vertical direction, or the air film thickness calibration, we synchronize both the RIM and TIRM techniques by using a lens with a known radius of curvature. The lens gives a calibration of the RIM method (fig. S1 (a)). A dove prism was specially ordered from Thorlabs to have both the top and bottom surfaces polished in order for synchronization of the two cameras. The lens resting on the prism surface automatically gives us a grayscale intensity that registers as a zero air film thickness from the TIRM side and also gives the absolute zero air film thickness for the initial dark fringe observed from the RIM side. When we lift the lens from the prism surface, the change in the air film thickness corresponds to a grayscale intensity trace on the TIRM side and a fringe-to-fringe spacing change on the RIM side.

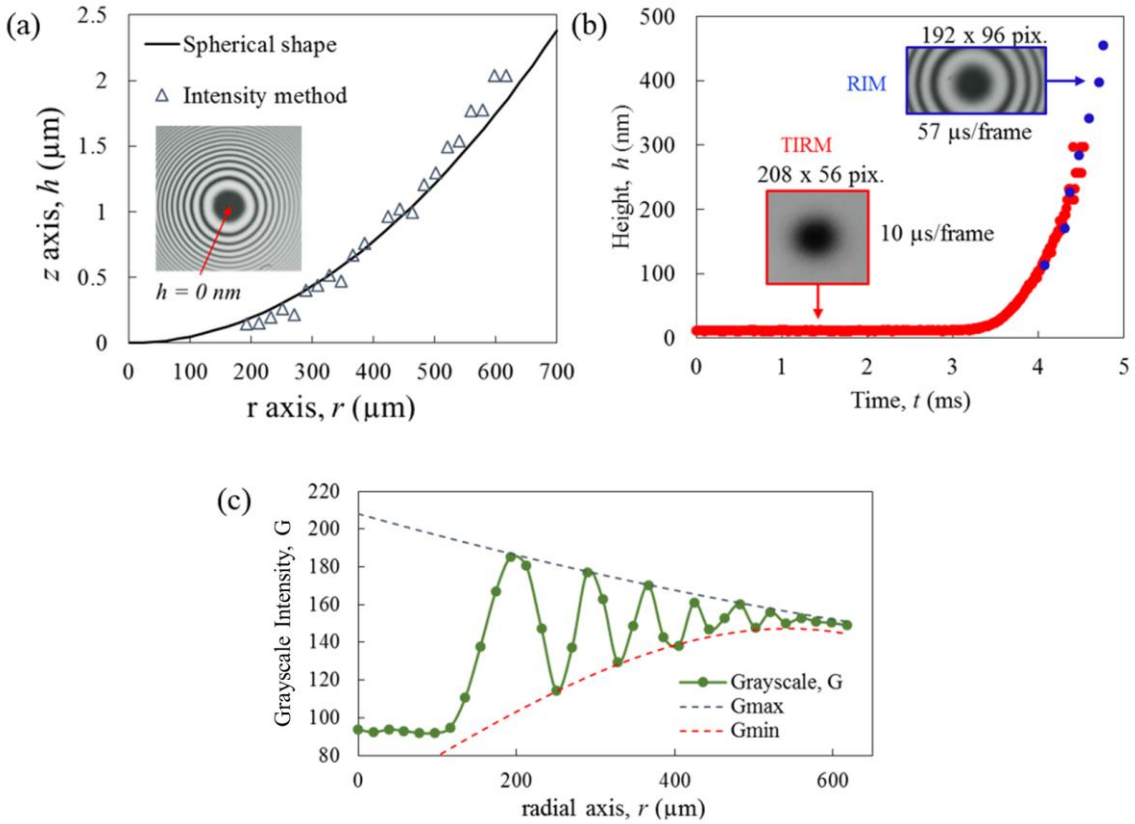

Fig. S1. Synchronized calibration of RIM and TIRM. (a) Calibration of the RIM method using a lens with a known radius of curvature (b) The air film thickness as a function of time for RIM and TIRM with synchronized signals. (c) an example grayscale intensity trace with respect to radius of the lens and the polynomial fitting used in the RIM method.

1.4 Combined TIRM-RIM technique

In order to determine the complete air profile underneath the falling drop, both the TIRM and RIM techniques were used for the TIRM-RIM method. The premise of this method lies in the fact that TIRM data sets the absolute film thickness on the order of ~100 nm and the RIM data provides the air film thickness on the order of a few microns. When the dimple profile determined by using RIM and the evanescence wave-derived air profile are combined, there is generally a slight offset in h where the first inflection point in the dimple height, H_d, otherwise denoted as the kink height H_k are matched. The H_k derived from RIM is then adjusted to meet the H_k derived from TIRM which causes the RIM data to shift downward (fig. S2 (a)). The RIM is used to observe the initial collapse of the dimple and the TIRM data is used to observe the minimal air film

thickness and to derive the contact time (Fig. S2).

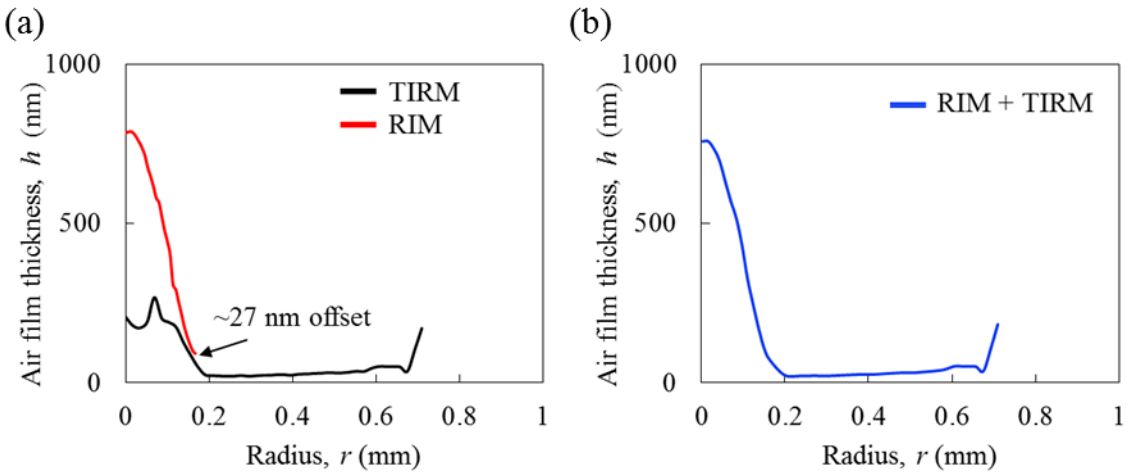

Fig. S2. The TIRM-RIM method (a) the TIRM and RIM methods separately measuring the air film morphologies (b) the combined TIRM and RIM method.

2. Oil film thickness measurement

The oil films were prepared by spin coating (Laurell) where the film thicknesses were verified via reflectometry (Filmetric F-20) based on the mismatch of the refractive index and weight measurement on a digital balance with an accuracy of 0.001 g (Denver Instrument) (fig. S3). The oil films were kept at $\approx 5\,\mu m$ using silicone oils (Sigma Aldrich) with viscosities of 4.56 to 970 cP. The films were made on #1 float glass coverslips from Chemglass (CLS 25mm×75mm).

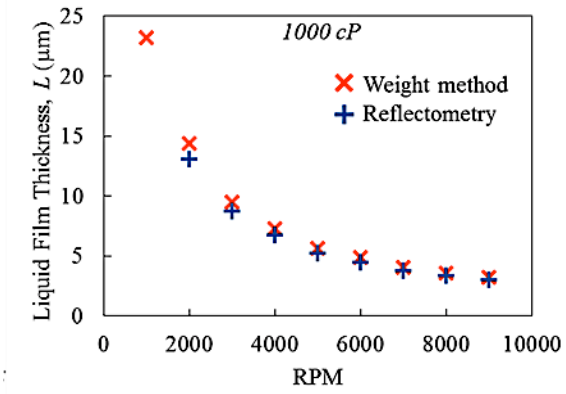

Fig. S3. Measurements of the oil film thickness based on weight and reflectometry methods.

3. Kink height measurement

Fig. S4 shows the minimum air film thickness, i.e., the kink height H_k as a function of the dimensionless time t/τ for varying We where τ is the inertial-capillary time scale defined as $\tau \equiv \sqrt{\rho_l R^3 / \sigma}$. As shown in fig. S4, the kink height drops rapidly upon impact (t = 0) and then slowly changes until it suddenly drops to zero. The rapid drop to zero at the later stage represents the rupture of the air film. The H_k value prior to rupture was used to determine critical height prior to rupture.

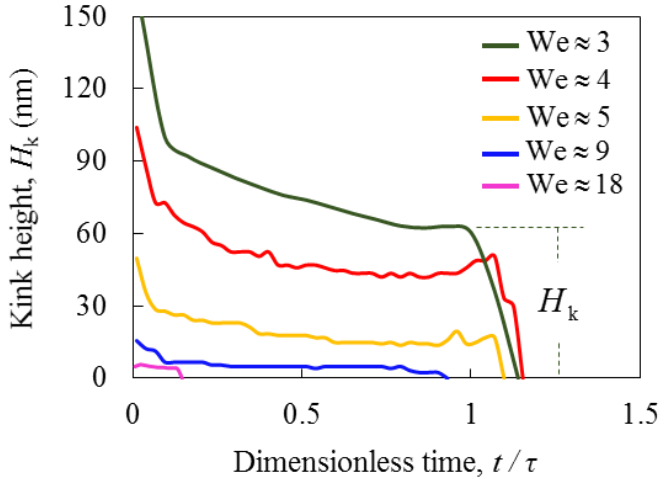

Fig. S4. The kink height, H_k as a function of dimensionless time t/τ.

References

[1] KOLINSKI J. M., MAHADEVAN L. and RUBINSTEIN S. M., *Phys. Rev. Lett.*, **112** (2014) 134501.

[2] DE RUITER J., MUGELE F. and VAN DEN ENDE D., *Phys. Fluids*, **27** (2015) 012104.

[3] VAN DER VEEN R. C., TRAN T., LOHSE D. and SUN C., *Phys. Rev. E*, **85** (2012) 026315.

[4] DE RUITER J., VAN DEN ENDE D. and MUGELE F., *Phys. Fluids*, **27** (2015) 012105.